JTTEES 7:181-190

PEER REVIEWED

Study of the Performance of TBC under Thermal Cycling Conditions using an Acoustic Emission Rig

J. Voyer, F. Gitzhofer, and M.I. Boulos

(Submitted 11 August 1997; in revised form 8 February 1998)

An experimental rig based on the use of infrared quartz lamps has been developed to monitor the degradation mechanisms causing failure of thermal barrier coatings (TBC) under thermal-cycling conditions. An acoustic emission (AE) technique monitored these degradation mechanisms, and advanced signals processing identified the key parameters that classify the AE signals according to the long-term behavior of the TBC. The AE technique enabled the localization of degradation sources inside the TBC with a linear resolution of ~5 mm by the use of two transducers fixed at both ends of the sample. Furthermore, sample zones of high AE activity showed typical vertical cracks at the surface and delaminations at the interface between the ceramic and the bond-coat layer. Vertical cracks were induced preferentially during the heating period of the thermal cycles when the ceramic coating was in a tensile-stress state, while delaminations were induced during the cooling period when the TBC was in a compressive-stress state.

Keywords acoustic emission, degradation mechanisms, thermal barrier coatings, thermal cycling, thermal stress

1. Introduction

In order to understand and characterize the failure of thermal barrier coatings (TBC) used in gas-turbine applications, an experimental thermal shock test rig reproducing thermal conditions encountered inside a turbine combustion chamber was developed to monitor the degradation mechanisms causing failure of TBC under thermal-cycling conditions. Because TBC failure is caused principally by thermal cycling (Ref 1), twelve infrared lamps with a power rating of 1.2 kW each were used as the heat source of the rig, producing a total thermal-heat flux on the sample surface of the order of 200 kW/m^2. The lamp mounting was backed by a highly reflective gold-coated water-cooled mirror, which concentrated the radiative energy onto the sample.

The sample was inserted in a quartz tube to perform the thermal tests under a controlled inert atmosphere to eliminate oxidation-related cracking phenomena. The TBC sample surface temperature was monitored by an infrared pyrometer.

Two ultrasonic transducers were fixed at both ends of the sample to detect the degradation mechanisms of the TBC by acoustic emission (AE) monitoring (Ref 2-7). The disposition of the two transducers enabled the determination of the linear location of the AE sources emitted from the sample. Furthermore, AE signal analysis was used to provide a way to predict the long term behavior of the TBC under thermal-cycling conditions. More details about the experimental setup are presented in Ref 8 and 9.

J. Voyer, F. Gitzhofer, and **M.I. Boulos,** CRTP, Dept. Chemical Engineering, Université de Sherbrooke, 2500 boul. Université, Sherbrooke, Québec, Canada J1K 2R1. Present address: J. Voyer, IMI-CNRC, 75 boul. de Mortagne, Boucherville, Quebec, Canada J4B 6Y4. Contact e-mail: joel.voyer@nrc.ca.

2. TBC Spraying Conditions

The samples investigated consisted of an INCONEL 625 substrate, 370 mm long, 25 mm wide, and 750 μm thick with a 100 mm central section covered with a duplex TBC, which consisted of an air plasma sprayed (APS) NiCrAlY bond-coat layer underneath an APS 20% yttria-stabilized zirconia (YSZ) coating. Table 1 lists the powders used for the plasma spraying of the TBCs.

Before the deposition of the bond-coat layer, the substrate was grit blasted with alumina particles of 240 grit size in compressed air flow. Following this grit blast, the substrate was ultrasonically cleaned to eliminate potentially included alumina grit blast media. In order to minimize the oxidation of the highly reactive substrate surface, the bond-coat layer was plasma sprayed within an hour after the grit blast.

Table 2 shows the plasma-spraying conditions of the NiCrAlY bond coat and the YSZ ceramic layer. An air barrier was used to avoid overheating the substrate during spraying of both layers. Following this bond-coat spraying, the YSZ coating was plasma sprayed with the conditions presented in Table 2, and finally, the samples were ultrasonically cleaned again. Spraying conditions of the bond coat and the ceramic layers (Table 2) are typical conditions used in the TBC aerospace industry.

Table 1 Type and composition of powders used for the fabrication of the TBC samples

Layer	Type	Composition	Particle size
Bond coat, NiCrAlY	Amdry 962(a)	67%Ni-22%Cr-10%Al-1%Y	-90 μm + 30 μm
Ceramic, YSZ	Amdry 146(a)	ZrO_2 + 20wt% Y_2O_3	-106 μm + 10 μm

(a) Sulzer Metco, Westbury, NY

Five different TBC samples were produced to evaluate their performance under thermal-cycling conditions. Table 3 summarizes the thickness and porosity values of these samples and indicates that the effect of the thickness of the ceramic layer, as well as the presence of a bond-coat layer on the performance of the TBC, was studied. Samples 4a and 4b (bond coat only) enabled the determination of the layer from which the AE signals are emitted,that is, it was possible to assess whether AE signals come from the ceramic layer or the bond-coat layer. As shown in Section 5, the AE signals emitted by the bond coat are shorter in duration and weaker in amplitude than the signals emitted from the YSZ coating. Therefore, for the samples consisting of a bond coat and a YSZ layer, the signals from the bond coat did not change significantly any characteristics of the signals from the YSZ coating because they were hidden by the latter signals. The thickness and porosity values were determined by image analysis of TBC optical micrographs. The porosity is an average of ten measures consisting of the ratio of pore area over the total area of the micrograph. The porosity values obtained are typical of APS YSZ coating. This high porosity value can increase the thermal durability of a TBC because the Young's modulus of a porous material is lower than for a dense material. Furthermore, the presence of pores can stop crack propagation (Ref 10).

Table 2 Plasma spraying conditions of the bond coat and the ceramic layers of TBC

Parameter	YSZ ceramic, NiCrAlY bond coat
Primary plasma gas, Ar, slpm at 50 psi	43
Secondary plasma gas, H_2, slpm at 50 psi	9.5
Powder gas, Ar, slpm at 50 psi	5
Powder feed rate, g/min	40 NiCrAlY, 55 YSZ
Power, kW	36
Current, A	400
Chamber pressure, Torr	760
Air barrier flow rate, slpm	9

Table 3 Parameters of the five TBC samples used for the thermal performance evaluation study

Sample	Bond coat, μm	Ceramic, μm	Porosity, %	Porosity standard deviation, %
1a, 1b	130	115	26.1	2.2
2a, 2b	130	160	26.8	7.9
3a, 3b	130	510	33.5	4.1
4a, 4b	130	...	...	...
5a, 5b	...	125	26.9	3.4

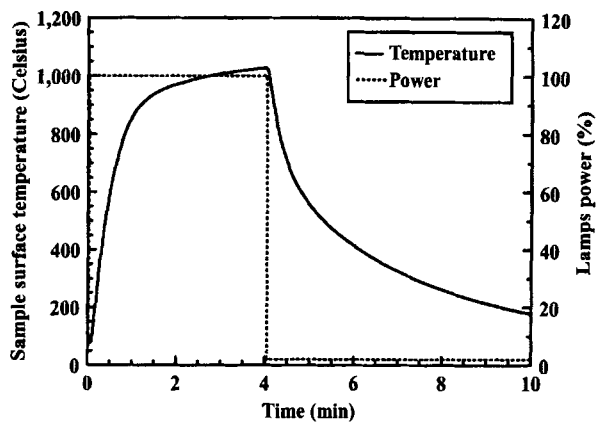

Fig. 1 Typical thermal cycle and sample surface temperature profile

3. Testing Conditions

The performance of the TBC samples was evaluated under thermal-cycling conditions. The thermal cycles consisted of a four-minute heating period at full power of the infrared lamps followed by a six-minute cooling period without the lamps. Figure 1 shows a typical cycle for the surface temperature of the TBC sample. The sample temperature reaches ~1000 °C at the end of the heating period, which is representative of the TBC temperature encountered in gas turbine applications. At the end of the cooling period, the sample surface temperature falls to ~200 °C. Further details about the characteristics of the thermal cycles are presented in Ref 8 and 9.

The first duplicata of each TBC sample was exposed to the heat source until it failed or to a maximum of 500 thermal cycles. The failure criterion was debonding (spalling) of at least 10% of the total surface of the TBC, determined with a ruler. When the performance of the TBC was <500 cycles, or if the maximum number of 500 cycles was reached, the TBC was withdrawn from the thermal rig and another sample was inserted for the evaluation of thermal performance.

The second duplicata of the TBC samples was exposed to only 30 thermal cycles. This enabled assessment of the reproducibility of the AE signals in the early thermal cycles and also allowed identification of the AE signal parameters (emitted during early cycles) that could be related to the long-term behavior of the TBC samples. This AE parameter identification could lead to the prediction of performance of TBC, based on AE data from early thermal cycles.

Thermally exposed TBC samples were examined with an optical microscope to correlate the high AE activity zones with visually detected defects.

4. Signal Analysis

Signal analysis used for the comparative evaluation of the TBC samples is discussed in this paper. More details on the basic signal analysis, as well as on the acquisition parameters, are found in Ref 8 and 9. A major drawback of Fourier transform analysis for the calculation of the frequency components of a time signal is that time-related information is lost. In order to obtain both time and frequency information simultaneously, a technique called the adjustable-width, sliding-time window was used. This technique allows determination of the arrival times of the frequency components of the AE signals and has potential for the classification of AE signals.

The time-frequency analysis uses a rectangular time window of width Δt ($\Delta t >$ signal length) and calculates the power spectrum of this segment of the signal. This calculation is repeated a

number of times for complete analysis of the AE signal; that is, the time window is slid over the entire signal, as shown in Fig. 2. For a time window width, Δt, and an AE signal total time length, T, there are N power spectrums ($N = T/\Delta t$). The width of the sliding-time window gives the time resolution (number of power spectrums) and the frequency resolution. This frequency resolution depends on the number of points on which the Fourier transforms are applied and on the sampling frequency ($\Delta f = f_s/N_p$, where Δf is the frequency resolution, f_s is the sampling frequency, and N_p is the number of points inside the time window). Therefore, a high number of points in the time window (high N_p and high Δt) permits a better frequency resolution than using a low number of points because the sampling frequency is constant. On the other hand, a large time window (high Δt) allows only a low time resolution. Therefore, a compromise is needed for the width of the time window to have the optimal time and frequency resolutions.

From this signal analysis, three-dimensional (3D) graphs were drawn with power spectrums calculated and median times of each time window (t_1, t_2 ..., t_N), as shown in Fig. 3. The abscissa of this graph gives the frequency, the ordinate gives the median time of the sliding window, and the magnitude of the power spectrums (V^2 rms) is given by the gray scale (third axis). Figure 3 shows that some zones of high-power spectrum magnitudes (dark zones) exist. These dark zones were not present prior to 1.5×10^{-4} s because the AE signals begin 1.5×10^{-4} s after the onset of the oscilloscope acquisition (oscilloscope trigger time delay). The distribution of these dark zones may be relevant to the degradation mechanisms within the samples and can be used for the classification of AE signals. Image analysis was performed to identify the dark zones and to calculate the center of mass, the total area, and the shape factor of each of these zones. The center of mass (x-axis = frequency and y-axis = time) locates the exact position of the dark zones in the 3D graph and is related to the arrival time and to the peak frequency of the high magnitudes of the signal. The total area is related to the magnitude of the AE signal and, therefore, to the magnitude of the degradation mechanism producing the AE signal. A severe degradation was related to a dark zone with a high-total area. Finally, the shape factor is defined as the ratio between the area and the square of the perimeter of the zone (shape factor = 4πarea per(perimeter)^2). This parameter assesses an evaluation of the circularity of the dark zones of the 3D graphs.

5. Results and Discussion

5.1 Mass Loss of TBC Samples

Table 4 shows the mass loss of the TBC samples exposed to thermal cycles. All code "b" TBC samples were exposed to the maximum number of thermal cycles (500) without experiencing severe visual damages (spalling), except for sample 5b, which exhibited a severe spallation of the YSZ coating after only 235 thermal cycles. The spallation of the YSZ coating arose, presumably, due to the absence of a bond coat. Sample 2b exhibited minute spallation of the YSZ coating near an edge. Table 4 does not indicate any data for group 4 samples, which consist of only a bond coat. These samples were exposed to a total of 275 thermal cycles without experiencing any visual damage. Furthermore, during these thermal cycles, only 9 AE signals were detected compared to several hundreds for the other samples. The AE signals emitted from group 4 samples were quite different than the AE signals emitted from group 1, 2, 3, and 5 samples. The amplitude and the duration of the AE signals emitted from the bond coat are weak (<25 mV and <0.5 ms) compared to signals from the other samples (>25 mV and ~2 to 3 ms). These results indicate that AE signals are emitted from the YSZ coating of the TBC samples, no signals (or very few signals) are emitted by the bond-coat layer, and that the bond-coat layer does not undergo significant degradation, at least as detected from this AE experiment performed under non-oxidizing conditions.

Table 4 Mass loss of the five TBC samples used for the thermal performance evaluation study

Sample	Thermal cycles	Mass loss, %
1a	30	4.4
1b	500	6.5
2a	30	4.4
2b	500	11.8
3a	30	0.7
3b	500	1.1
5a	30	15.9
5b	235	37.5

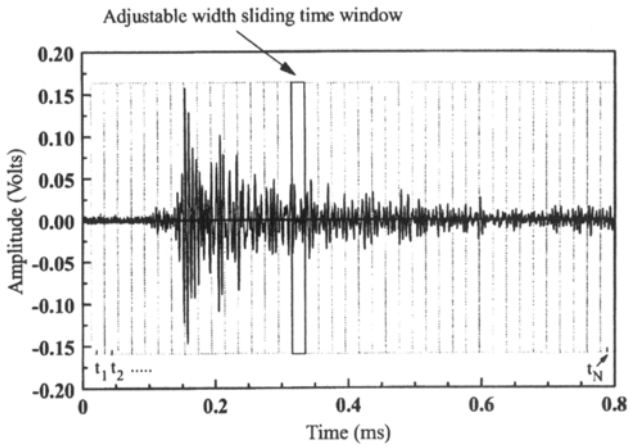

Fig. 2 Adjustable-width, sliding-time window analysis technique

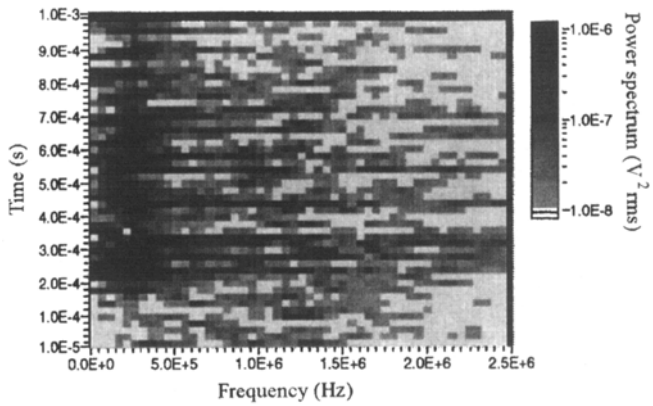

Fig. 3 Time-frequency 3D graph

5.2 3D Graph Analysis

As noted earlier, TBC samples with long durability should be discriminated from samples of short durability by the use of the 3D graph analysis. In this sense, the parameters extracted from 3D graphs of group 2 samples (long durability) and group 5 samples (short durability) were compared to identify any differences that could lead to the classification of AE signals. Figures 4 and 5 show the area distributions of samples 2 and 5. These distributions are quite similar because they share almost the same area range. It is difficult to discriminate the long durability TBC samples from the short samples by the total area distribution. The differences between duplicates of the same sample can be explained by the fact that duplicate a has undergone 30 thermal cycles; therefore, very few AE signals are emitted in comparison with duplicate b, which has undergone several hundred thermal cycles. The same conclusions drawn for the total area of the 3D graphs can be drawn for the distributions of the time center of mass, the distributions of the frequency center of mass, and the distributions of the shape factor. The remarkable similarity between the long durability TBC sample distributions and the short durability samples suggests that the AE signals emitted from these samples are identical. Furthermore, as noted earlier, it is not possible to discriminate AE signals emitted from long durability TBC samples from signals emitted by short durability samples by the analysis of the 3D graphs. These results have led the authors to analyze the cumulative AE number and the cumulative AE energy to differentiate TBC samples with different durabilities.

5.3 Cumulative Number of AE Signals

Figure 6 shows the cumulative AE number for each sample for the overall thermal cycles. It is shown that sample 1b emits ~100 AE signals for 500 cycles, sample 2b emits 750 signals after 500 thermal cycles, sample 3b emits 825 signals after 500 cycles, and sample 5b emits 260 signals after 235 cycles. Therefore, sample 3b has the highest AE activity followed by sample 2b, 5b, and 1b. Nevertheless, a high AE activity does not necessarily indicate a short TBC sample durability because two of the three most durable samples possess a high AE activity (2b and 3b). The cumulative AE number cannot be used to establish a correlation with the durability of the TBC samples because this

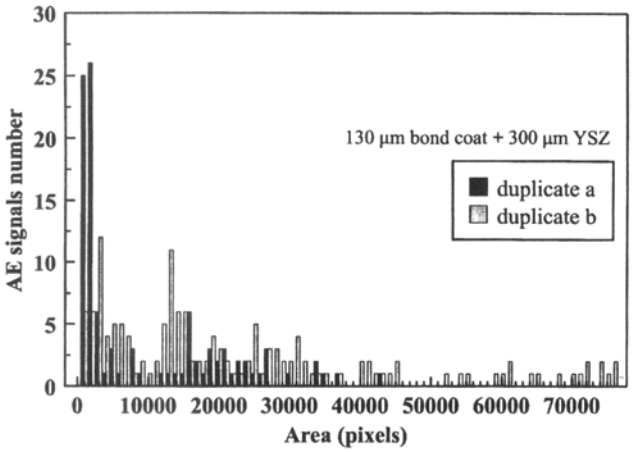

Fig. 4 Three-dimensional graph area distribution of sample 2

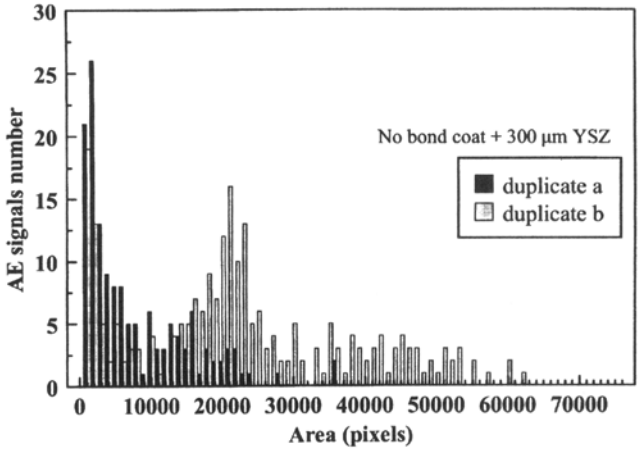

Fig. 5 Three-dimensional graph area distribution of sample 5

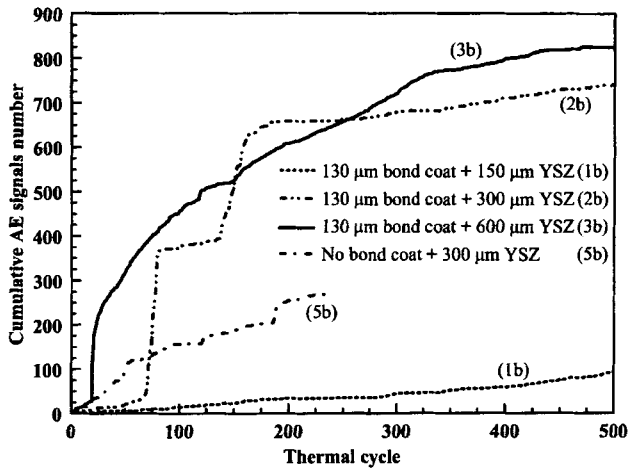

Fig. 6 Cumulative AE signals number emitted from thermal barrier coating samples for the overall thermal cycles

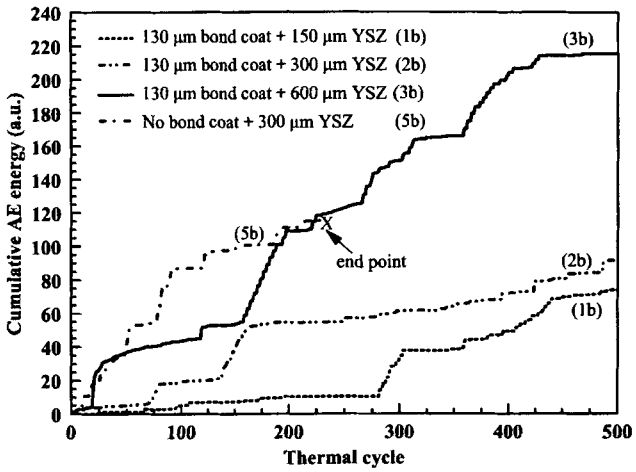

Fig. 7 Total cumulative AE energy emitted from thermal barrier coating samples for the overall thermal cycles

number represents the number of cracks or other sources that can give rise to AE behavior occurring in the TBC without representing the magnitude of these mechanisms. In fact, a TBC sample can develop a large number of very small cracks, which are not dangerous to integrity, or it can develop a few large cracks that can be deleterious. Therefore, the analysis of the cumulative AE energy is preferred to the cumulative number of AE signals and should be more indicative of the degradation mechanisms of the TBC samples.

5.4 Total Cumulative AE Energy

Figure 7 shows the total cumulative AE energy of the samples studied for the overall thermal cycles performed. It is shown that sample 1b emits around 75 a.u. (arbitrary units). of acoustic energy, sample 2b has a total energy of 90 a.u., sample 3b emits a total energy of 215 a.u., and sample 5b has an energy value of 115 a.u. after 235 thermal cycles. Sample 3b is the most acoustically energetic TBC sample, followed by samples 5b, 2b, and 1b. Samples 1b and 2b have similar characteristics (thickness ~150 μm and durability >500 thermal cycles), and these similarities are reflected in their total cumulative energy. Sample 3b has a thicker YSZ coating (~510 μm) than the other samples; this gives it the disadvantage of being more susceptible to thermal stresses. This sample has a high-acoustic energy emission and demonstrates that it experienced significant damage. This feature was confirmed later by optical microscopy. Even if sample 3b experienced some high-magnitude crack formation or propagation shown by the high AE energy, it still has a durability of >500 thermal cycles. This can be explained by the high thickness of sample 3b, which stops the onset of the macroscopic degradation because the AE energy density should be considered. Then, the comparison of the durability of the samples should account for the thickness of the samples. Furthermore, sample 3b possesses a higher porosity than the other samples (Table 3); this can play a role in increasing the TBC durability by blocking the crack propagation. Sample 5b has the shortest durability and emits a greater total cumulative AE energy compared to sample 2b, which has a similar thickness. The high AE energy of sample 5b confirms that it experienced significant cracking, as is shown by the loss of mass (Table 4).

Because thickness of the TBC sample played a role in their durability, the total cumulative AE energy was normalized for a YSZ coating thickness of 100 μm to compare the different samples (AE energy density).

Figure 8 shows the total cumulative AE energy normalized for a thickness of 100 μm. It shows that samples 1b, 2b, and 3b all have approximately the same AE energy after 500 thermal cycles (between 40 and 60 a.u./100 μm), and sample 5b emits twice as much (~95 a.u./100 μm) energy. Thus, the sample with the shortest durability, sample 5b, exhibits the highest normalized total cumulative AE energy. The other samples, which possess a higher similar durability, emit a similar normalized cumulative energy. From these results, it seems that a correlation exists between the durability of the TBC and the normalized total cumulative AE energy emitted from the TBC. Because the goal of this study is to establish a correlation of the durability of the TBC with the AE signals of early stages of the thermal tests, a more detailed analysis of the first 30 thermal cycles will be completed. This number of thermal cycles was chosen for the significant number of AE signals emitted (~10% of the total number of AE signals) and, therefore, a significant correlation of the AE signals of these early cycles with the durability of the TBC samples is achieved.

5.5 Total Cumulative AE Energy Emitted in the First 30 Thermal Cycles

Figure 9 shows the total cumulative AE energy normalized for a YSZ thickness of 100 μm of the samples for the first 30 thermal cycles. Once again, the sample with the shortest durability, sample 5b, exhibits the highest normalized AE energy (~20 a.u./100 μm) followed by the three other samples, which have longer durabilities (>500 cycles) and lower normalized energy (~3 a.u./100 μm). Therefore, the long term durability of the TBC samples can be predicted by the normalized total cumulative AE energy emitted during the first 30 thermal cycles.

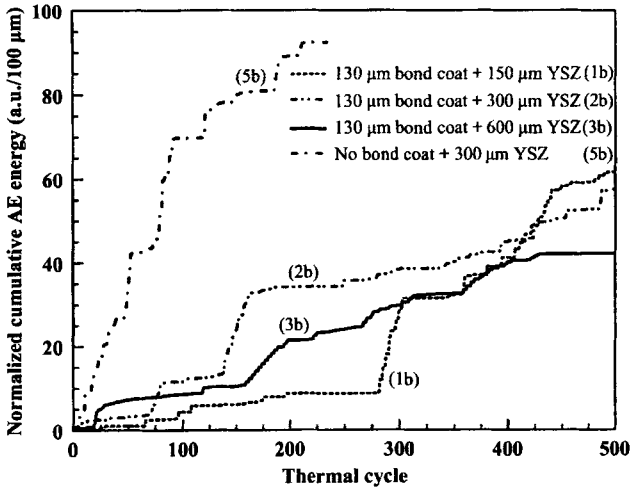

Fig. 8 Total cumulative AE energy emitted from thermal barrier coating samples normalized for a yttria-stabilized zirconia thickness of 100 μm for the overall thermal cycles

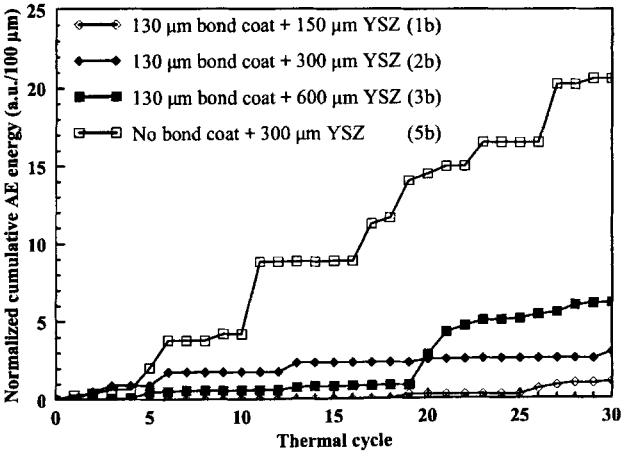

Fig. 9 Total cumulative AE energy emitted from thermal barrier coating samples normalized for a yttria-stabilized zirconia thickness of 100 μm for the first 30 thermal cycles

5.6 AE Signals Emitted during the Heating and Cooling Period

Because the heating and cooling periods of the thermal cycles represent different TBC stress states, further analysis has been performed to compare AE signals emitted during both periods. In fact, during heating periods, the TBC, as well as the metallic substrate, were heated by the infrared lamps. Because the metal had a higher thermal expansion coefficient than the TBC, the TBC was in a tensile-stress state. For the cooling periods, the metallic substrate was cooled by an argon jet directed on the back of the substrate. Therefore, the substrate cooled down more rapidly than the TBC, placing this substrate in a compressive-stress state.

Table 5 gives the number of AE signals emitted by each sample for the first 30 cycles and for the overall thermal cycles. Samples 1a, 1b, 2a, and 2b emit very few AE signals during the cooling periods of the first 30 cycles, and the heating periods of these first cycles are more ultrasonically active. This predominance of AE during the cooling period for the first 30 cycles changes to a predominance of AE during the heating period after 500 thermal cycles. This behavior is different from that of samples 3a and 3b, for which the cooling periods are the most ultrasonically active during all thermal cycles (after 30 and 500 cycles). Samples 5a and 5b have approximately equivalent cooling and heating periods for the first 30 thermal cycles. This changes for a more active cooling period when analyzing all thermal cycles. Table 5 also shows the ratio, normalized for a YSZ thickness of 100 μm, of the number of AE signals emitted in the cooling periods of the first 30 cycles over the total number of AE signals emitted during the same number of cycles. Samples with a long durability have a low ratio (~0.1 to 0.25), and the samples with a short durability have a high ratio. This ratio correlates to the long-term behavior (durability) of the TBC samples.

Table 6 presents the AE energy emitted during the cooling and heating periods of the first 30 and for the overall thermal cycles. This table is quite similar to Table 5. Samples 1 and 2 have significant emission of AE energy during the heating period of the first 30 cycles. At the end of the overall cycles, the behavior is reversed so that the cooling periods are more acoustically energetic than the heating periods. Sample 3 has more energetic cooling periods than heating cycles throughout the overall thermal cycles. The behavior for sample 5 is uncertain. The first duplicate a emits more acoustic energy during the cooling periods of the first 30 cycles and the second duplicate b emits more energy during the heating periods of the first 30 cycles. The behavior of duplicate b during the first 30 cycles changes, and at the end of all cycles, the cooling periods are more acoustically energetic than the heating periods, similar to duplicate a. The differences between these duplicates can be explained by the fact that even if they were plasma sprayed simultaneously, it is possible that the samples have slight differences in their characteristics. These small differences can result in a different thermally induced AE signals emission behavior and in a different thermal durability. Because sample 5b experienced severe degradation (spallation) after 235 thermal cycles and that the number and total energy of cooling AE signals are more important than those of the heating periods, it seems that a compressive-stress state is more deleterious for the TBC integrity than a tensile-stress state.

Table 5 Number of AE signals emitted during the cooling and heating periods of the first 30 and the overall thermal cycles

Sample	Heating AE signals, 30 cycles	Cooling AE signals, 30 cycles	Heating AE signals, total cycles	Cooling AE signals, total cycles	C/T per 100 μm, 30 cycles	Durability
1a	5	2	...	...	0.24	>30
1b	5	1	35	57	0.14	>500
2a	16	3	...	...	0.10	>30
2b	14	0	325	418	0	>500
3a	41	185	...	...	0.16	>30
3b	70	178	327	499	0.14	>500
5a	23	27	...	...	0.43	>30
5b	25	19	55	105	0.34	235

C/T is the ratio of the number of AE signals emitted in the cooling periods of the first 30 thermal cycles over the total number of AE signals emitted in the first 30 thermal cycles.

Table 6 AE energy emitted during the cooling and heating periods of the first 30 and the overall thermal cycles

Sample	Heating AE energy(a), 30 cycles	Cooling AE energy, 30 cycles	Heating AE energy, total cycles	Cooling AE energy, total cycles	C/T per 100 μm, 30 cycles	Durability
1a	5.93	0.041	...	...	0.006	>30
1b	1.26	0.028	17.7	56.4	0.018	>500
2a	6.16	0.630	...	...	0.058	>30
2b	3.03	0	18.0	29.0	0	>500
3a	31.2	115.0	...	...	0.154	>30
3b	3.52	27.70	48.3	167	0.174	>500
5a	1.17	6.850	...	...	0.683	>30
5b	15.0	10.70	18.3	41.3	0.333	235

C/T is the ratio of the AE energy emitted in the cooling periods of the first 30 thermal cycles over the total AE energy emitted in the first 30 thermal cycles. (a) Energy is in arbitrary units.

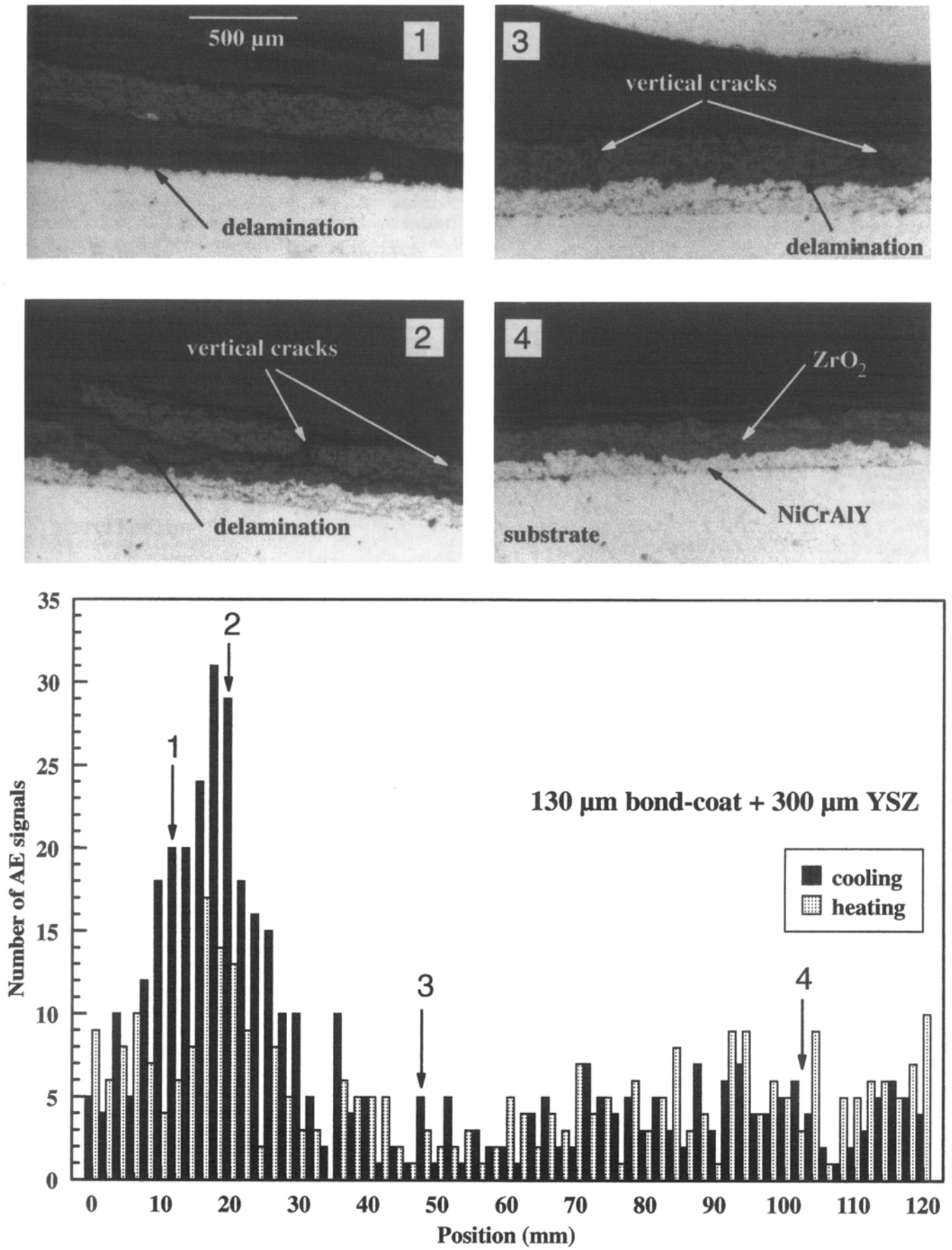

Fig. 10 Optical micrographs and position distribution of AE signals emitted by sample 2b during the overall thermal cycles

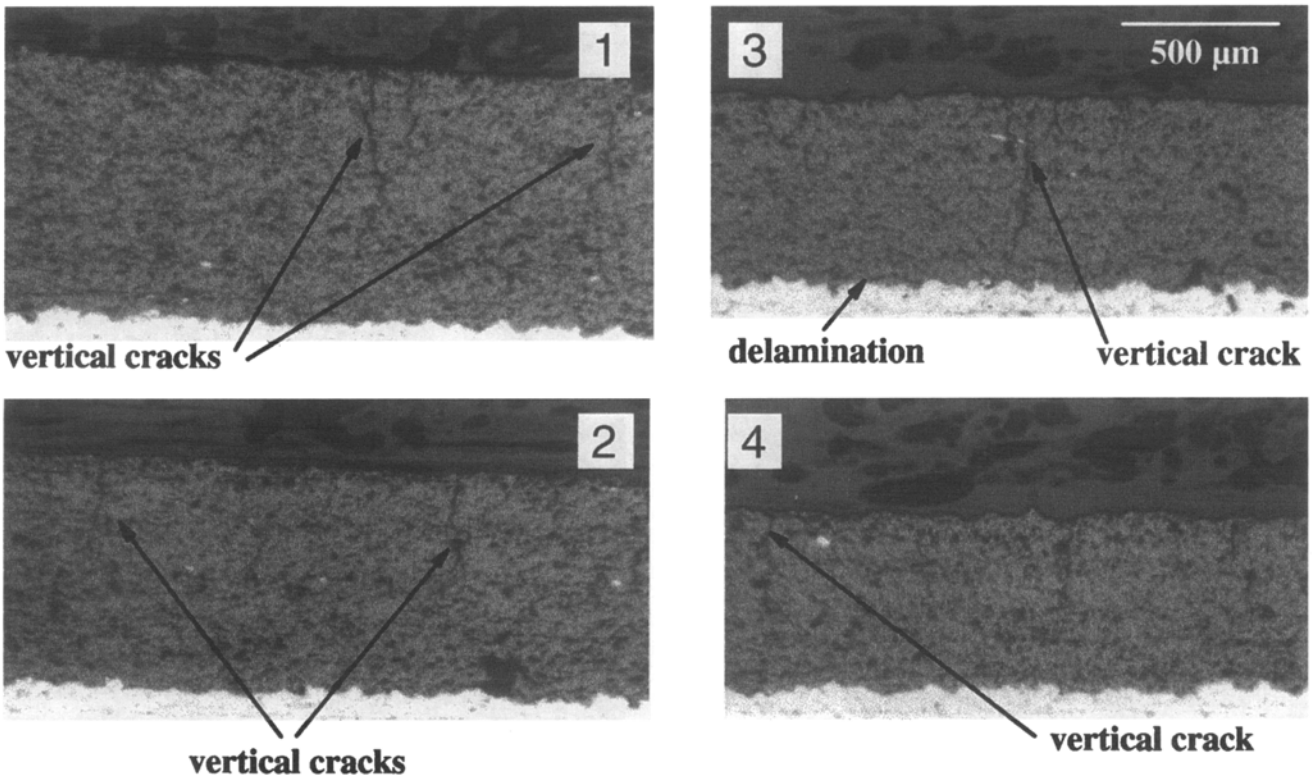

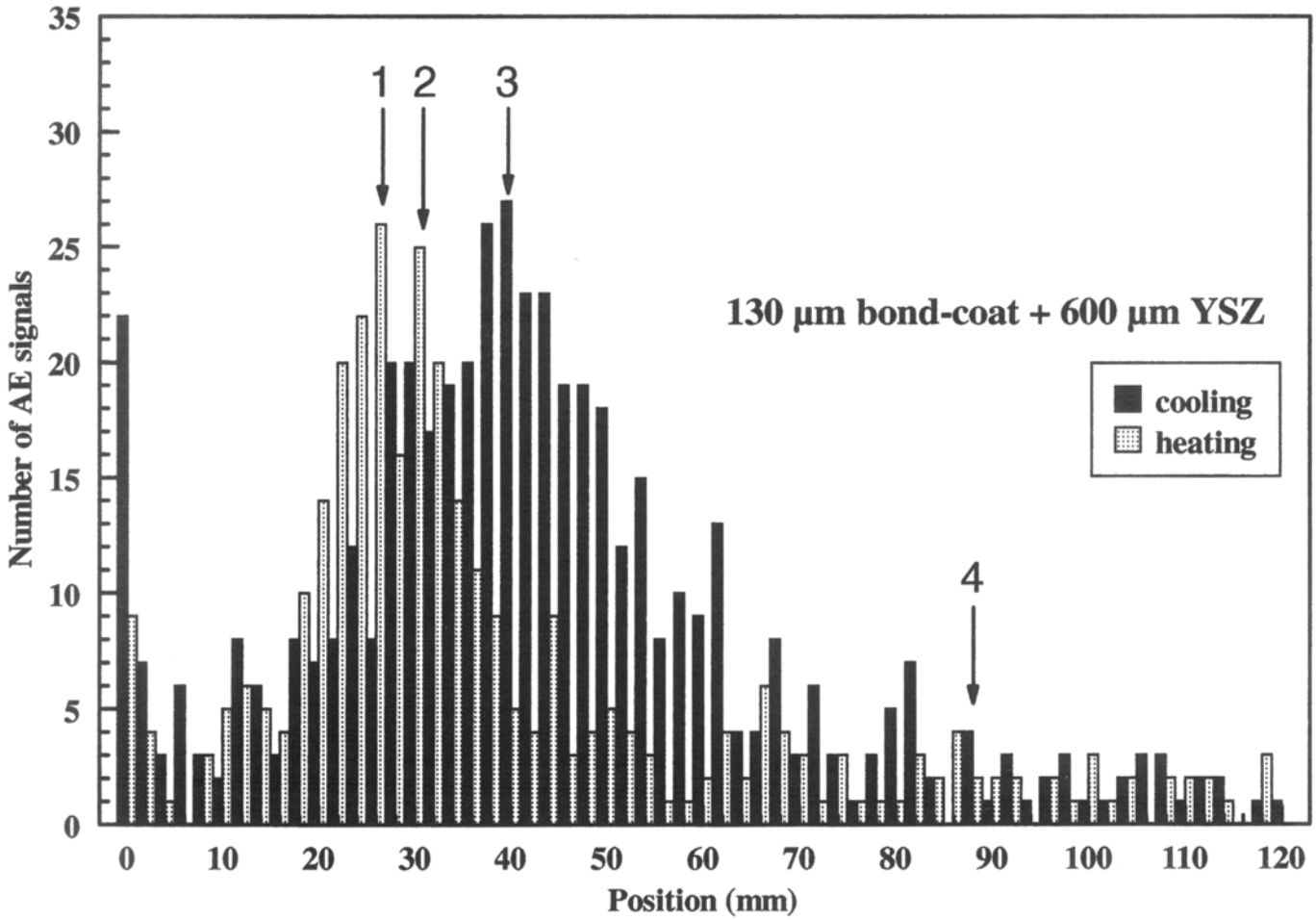

Fig. 11 Optical micrographs and position distribution of AE signals emitted by sample 5b during the overall thermal cycles

The tensile-stress state helps the formation of perpendicular (to the interface between the YSZ and the bond-coat layer) surface cracks, and the compressive-stress state produces near-interface cracks that can develop into delaminations of the YSZ (Ref 11, 12). These near-interface cracks occur in the YSZ coating parallel and very close (a few μm) from the interface between the YSZ and the bond-coat layer (Ref 13). These interface cracks can produce a partial or total spalling of the TBC (Ref 13).

From the results for samples 1 and 2 from Tables 5 and 6, it appears that perpendicular surface cracks are produced for the first time; afterwards, the formation of near-interface cracks occurs. The presence of surface cracks increases the tensile-stress value along the sample thickness, helping the initiation of near-interface cracks (Ref 12). Table 6 also gives the ratio normalized for a YSZ thickness of 100 μm of the AE energy emitted during the cooling periods over the total energy emitted during the first 30 thermal cycles. Again, this ratio gives a good indication of the TBC durability. Thus, the samples with a short durability (sample 5) have a high ratio, that is, more AE energy is emitted during the cooling periods of the thermal cycles than in the heating periods. This means that these samples potentially possess deleterious near-interface cracks that give rise to possible macroscopic delaminations.

5.7 Location of AE Signals

As noted earlier, the disposition of the two ultrasonic transducers enables the localization of the thermally induced degradation mechanisms in the TBC. Figure 10 shows the position distribution of sample 2b for the cooling and heating periods of the overall thermal cycles. The abscissa represents the entire length of the TBC coating. A zone of high AE activity exists in the range from 10 to 30 mm. This high AE activity zone coincides with the location of cracks, as shown in Fig. 10. Figure 10(a) (micrograph 1) shows a delamination of the ceramic layer due to the absence of a bond-coat layer. This is probably due to a misalignment of the sample with regard to the direct current (dc) plasma-spray gun during the projection of the sample. This error left the edge of the metallic strip uncovered by a bond coat; this results in a delamination of the ceramic layer.

Figure 10(b) (micrograph 2) shows a delamination combined with vertical surface cracks. Note that these cracks coincide with the maximum AE activity of both the cooling and heating period. Figure 10(c) and (d) (micrographs 3 and 4) are taken from low AE activity, and these zones do not reveal severe degradation mechanisms because no important cracks are visible. These results confirm that the cooling period of the cycles puts the TBC into a compressive-stress state, that the heating period produces a tensile-stress state, and that tensile stress predominantly induces vertical cracks at the surface of the TBC, while compressive stress induces delamination of the YSZ coating near the interface between the ceramic coating and the bond-coat layer, where the bond strength is weaker. Figure 10(e) shows that delamination is centered around the maximum AE activity of the cooling period, and the vertical cracks at the surface of the TBC are centered in the vicinity of the maximum AE activity of the heating period.

Figure 11 shows a position distribution and optical micrographs for sample 3b. Again, it is clearly seen from the micrographs and the distribution that the cooling period of the thermal cycles preferentially induces delaminations at the interface, while the heating period of the cycles preferentially induces vertical cracks at the surface of the ceramic coating. Vertical cracks and delaminations observed in the samples studied may have occurred in locations where some defects are present: aligned pores, ceramic bond-coat adhesion defects, splats interfaces, etc.

6. Conclusions

The AE technique has shown that the AE signals are emitted from the YSZ coating only, and that the bond-coat layer does not degrade under thermal cycling in an inert atmosphere. This technique can localize thermally induced cracks within TBC samples with a linear resolution of ~5 mm.

The adjustable-width, sliding-time window analysis technique was not able to discriminate the AE signals emitted from TBC with short lifetime from the signals emitted by TBC with long-term thermal-cycling history.

High AE activity zones were shown to be the source of cracks in the TBC. Furthermore, this technique can discriminate between vertical cracks at the surface and delaminations of the interface by analysis of the AE signals emitted during the heating and the cooling period of the thermal cycles. Vertical surface cracks were produced by a tensile-stress state during heating periods, and the near-interface cracks were initiated by a compressive-stress state during cooling periods of the thermal cycles.

The long term behavior (durability) of the TBC can be related to three parameters extracted from the first 30 thermal cycles:

- Total cumulative AE energy normalized for a YSZ thickness of 100 μm
- Ratio normalized for a YSZ thickness of 100 μm of the number of AE signals emitted during the cooling periods compared to the total number of AE signals
- Ratio normalized for a YSZ thickness of 100 μm of the AE energy emitted during the cooling periods compared to the total AE signal energy

A more detailed statistical analysis for an important number of TBC samples will enable a precise correlation between one or more of these three parameters and the durability of the TBC.

Acknowledgments

This project was funded by the Natural Sciences and Engineering Research Council of Canada and Pratt & Whitney Canada through a university-industry collaboration research program. The financial support by the Ministère de l'Éducation of the Province of Québec through its FCAR-Scholarship to Mr. J. Voyer is gratefully acknowledged.

References

1. K.D. Sheffler and D.K. Gupta, Current Status and Future Trends in Turbine Application of Thermal Barrier Coatings, *J. Eng. Gas Turbines Power (Trans. ASME)*, Vol 110, 1988, p 605-609
2. C.C. Berndt, Acoustic Emission Evaluation of Plasma-Sprayed Thermal Barrier Coatings, *J. Eng. Gas Turbines Power (Trans. ASME)*, Vol 107, 1985, p 142-146

3. D.M. Romrell and L.R. Bunnell, Monitoring of Crack Growth in Ceramic by Acoustic Emission, *Materials Evaluation,* Society for Nondestructive Testing, 1970, p 267-276
4. N.R. Shankar, C.C. Berndt, and S. Rangaswamy, Acoustic Emission from Thermally Cycled Plasma-Sprayed Oxides, *Ceram. Bulletin,* Vol 62 (No. 5), 1983, p 614-619
5. C.C. Berndt and H. Herman, Failure during Thermal Cycling of Plasma-Sprayed Thermal Barrier Coatings, *Thin Solid Films,* Vol 108, 1983, p 427-437
6. C.C. Berndt, Failure Processes within Ceramic Coatings at High Temperatures, *J. Mater. Sci.,* Vol 24, 1989, p 3511-3520
7. C.C. Berndt and R.A. Miller, Failure Analysis of Plasma-Sprayed Thermal Barrier Coatings, *Thin Solid Films,* Vol 119, 1984, p 173-184
8. J. Voyer, F. Gitzhofer, M.I. Boulos, and S. Durham, Thermally Induced Acoustic Emissions in Thermal Barrier Coatings, *Thermal Spray Science & Technology,* C.C. Berndt and S. Sampath, Ed., ASM International, 1995, p 457-462
9. J. Voyer, "Étude d'Émission Acoustique de Barrières Thermiques sous des Conditions de Chargement Thermique Cyclique," Ph.D. thesis, Université de Sherbrooke, 1997 (in French)
10. D.L. Ruckle, Plasma-Sprayed Ceramic Thermal Barrier Coatings for Turbine Vane Platforms, *Thin Solid Films,* Vol 73, 1980, p 455-461
11. M. Enoki, T. Kishi, and T. Mantyla, Characterization of Microfracture in Coatings during Thermal Shock Test using Acoustic Emission, *Proc. 3rd Japan Int. SAMPE Symposium,* 1993, p 2335-2340
12. Y.R. Takeuchi and K. Kokini, Thermal Fracture of Multilayer Ceramic Thermal Barrier Coatings, *J. Eng. Gas Turbines Power (Trans. ASME),* Vol 116, 1994, p 266-271
13. P. Dionne and S. Roberge, "Plasma Spray Process for High Performance Thermal Barrier Coatings," Pratt & Whitney Canada Technical Report ER-2764, 1993